Lens-Enabled Beam Selection under IFTR Fading: Optimal Rate Analysis and Design Insights

Hui Zhao[a,*], T. Q. Khai Nguyen[b] and Dirk Slock[a]

[a]Communication Systems Department, EURECOM, 06410 Sophia Antipolis, France
[b]Thales Research & Technology, 91120 Palaiseau, France

ARTICLE INFO

Keywords:
Beamforming
Fluctuating two-ray fading
Lens antenna
mmWave

ABSTRACT

We study the effective transmission rate (ETR) optimization for lens-enabled beam selection with a single radio-frequency (RF) chain over independently fluctuating two-ray (IFTR) fading channels. A high-SNR asymptotic outage probability (OP) yields a low-complexity closed-form approximation to the signal-to-noise ratio (SNR) threshold that maximizes the ETR, while the exact Gamma-mixture representation provides a benchmark for assessing the design accuracy. An exact stationary condition, a second-order high-SNR expansion, and a local curvature analysis characterize the threshold design and its resulting ETR loss. For the unusually large measurement-fitted K-factor, the physical IFTR parameters are retained in all performance evaluations, while a moderate K_s is used only as a design surrogate. Monte Carlo channel simulations validate the analytical ETR results, while numerical evaluation of the exact IFTR Gamma-mixture representation quantifies the ETR loss of the proposed threshold design relative to the exact optimum. A representative fixed choice $K_s = 15$ keeps this loss below 2.5% at the tested 0–30 dB average SNRs for the fitted channel. Finally, full-wave electromagnetic (EM) patterns of a fabricated dielectric lens are incorporated into the link evaluation. For eight transmit feeds or array elements and a transmit SNR of 0 dB, the lens architecture achieves a higher optimal ETR than the ideal analog-beamforming reference with the same element count within a $\pm 30°$ sector, with a boresight ratio exceeding three.

1. Introduction

Millimeter-wave (mmWave) spectrum helps relieve sub-6 GHz congestion and offers wide bandwidths and large-array opportunities [1, 2, 3, 4]. Compared with sub-6 GHz, however, mmWave signals suffer much stronger propagation loss. Multi-antenna arrays and beamspace transmission can form narrow, directional beams to counter this loss and improve spectral efficiency [3, 5], but operating at tens of gigahertz drives up hardware cost and power consumption. Even hybrid beamforming—with far fewer radio frequency (RF) chains than antennas—still carries substantial front-end overhead at mmWave [3]. To reduce hardware complexity and power consumption, single-RF-chain transmission has attracted increasing attention [6, 7, 8]. In such systems, beamforming is typically realized through per-antenna phase shifters, which still incur non-negligible power consumption. This motivates the design of low-complexity beamforming architectures that avoid dense phase-shifter networks while maintaining efficient directional transmission, among which lens-enabled front-ends provide a practical solution by enabling beam steering via antenna selection without per-antenna phase shifters [9, 10, 11, 12].

In practical mmWave environments, small-scale channel fading is usually characterized by strong specular components together with diffuse scattering. The fluctuating two-ray (FTR) model [13] captures this structure through two dominant specular components with common amplitude fluctuations and a diffuse component, and has demonstrated improved fitting accuracy over several conventional fading models when compared with outdoor far-field 28-GHz measurement data [14]. The independently fluctuating two-ray (IFTR) model [15] further extends this framework by allowing the two specular components to fluctuate independently, and numerical evaluations have demonstrated its improved modeling accuracy for mmWave channels. However, the analytical complexity of FTR and IFTR fading has historically hindered their use in system-level performance analysis and engineering design [16, 17, 18, 19]. Although recent advances, particularly the Gamma-mixture representation of the IFTR distribution [20], have enabled tractable evaluation of several performance metrics, deriving simple analytical rules for performance optimization under IFTR fading remains challenging. More recently, the delay-constrained throughput performance of multiple-input single-output (MISO) systems over IFTR fading has been investigated under statistical delay constraints [21]. However, this metric differs from the effective transmission rate (ETR) considered in this work. Here, the ETR is defined as the product of the successful-transmission probability and the target spectral efficiency. It therefore captures the tradeoff between increasing the decoding signal-to-noise ratio (SNR) threshold to support a higher target spectral efficiency and the resulting increase in outage probability (OP). This tradeoff makes the decoding SNR threshold a key design variable for ETR maximization.

While lens-enabled beamforming architectures based on feed selection have attracted considerable attention, most existing performance analyses rely on classical fading models. Their behavior under more accurate models such as FTR

*Corresponding author
hui.zhao@eurecom.fr (H. Zhao);
tran-quang-khai.nguyen@thalesgroup.com (T. Q. Khai Nguyen);
dirk.slock@eurecom.fr (D. Slock)
ORCID(s):

and IFTR fading therefore remains insufficiently understood. Moreover, although a high-SNR asymptotic OP is available for IFTR fading [15, 20], its use for ETR optimization is nontrivial because the decoding threshold varies with the operating SNR. The difficulty is amplified for the unusually large measurement-fitted K-factor considered here, for which convergence of the asymptotic OP to the exact OP is slower over practical finite-SNR ranges [15]. These observations motivate a tractable ETR-maximizing threshold rule together with an exact benchmark and an explicit assessment of its finite-SNR design accuracy.

In this paper, we study a lens-enabled transmit beamforming architecture for mmWave communications over an IFTR fading channel. A single feed illuminates the lens at a time, and feed selection determines the transmit beam direction and the corresponding beamforming gain. The main contributions are summarized as follows.

- We formulate the received SNR for both single-RF-chain analog (AG) beamforming and the lens-enabled architecture using the same IFTR fading model, with their respective beamforming gains explicitly included. Using the high-SNR asymptotic OP, we derive a low-complexity closed-form rule for the ETR-maximizing decoding threshold. The exact Gamma-mixture distribution then provides the exact ETR benchmark and the stationarity condition for its maximization.
- We characterize the validity and accuracy of the asymptotic design. A second-order expansion quantifies the deviation from the high-SNR asymptotic OP, we show that the normalized threshold tends to zero even though the ETR-maximizing threshold grows with SNR (cf. Remark 2). This justifies applying the high-SNR OP expansion along the designed threshold. A local curvature result then quantifies how a small threshold error translates into ETR loss.
- For the extremely large measurement-fitted K-factor, directly applying the high-SNR closed-form threshold rule can lead to substantial ETR loss at practical SNRs. We therefore introduce a moderate-K surrogate for threshold design while retaining the fitted IFTR model for performance evaluation. Numerical results quantify the threshold error, ETR loss, and sensitivity to both the surrogate choice and the physical IFTR parameters.
- We incorporate full-wave electromagnetic (EM) radiation patterns of a fabricated dielectric lens into the link evaluation. Both architectures use a single transmit RF chain, the same number of lens feeds or AG array elements, and the same total transmit power, with beam steering achieved through lens-feed selection or AG phase control, respectively. We identify the angular region in which the lens architecture achieves a higher ETR than the ideal AG reference. This comparison is distinguished from an equal-aperture or equal-effective-isotropic-radiated-power (EIRP) hardware comparison.

The remainder of this paper is organized as follows. Section 2 introduces the AG and lens-enabled architectures together with the normalized IFTR channel model. Section 3 develops the low-complexity asymptotic ETR design, while Section 4 establishes the exact Gamma-mixture benchmark and quantifies the approximation error. Section 5 assesses the extreme-K surrogate design and physical-parameter sensitivity, then combines the statistical model with full-wave EM lens patterns for the system-level comparison. Finally, Section 6 concludes the paper.

Notations. We use $\mathbb{C}$ to denote the set of complex numbers, and $\jmath \triangleq \sqrt{-1}$ is the imaginary unit. $|\cdot|$ denotes the magnitude of a complex number, while $\|\cdot\|$ denotes the Euclidean norm. $\mathbb{E}\{\cdot\}$ denotes the expectation operator. For a matrix $\mathbf{A}$, $\mathbf{A}^T$, $\mathbf{A}^*$ and $\mathbf{A}^H$ represent its non-conjugate transpose, element-wise conjugate and conjugate transpose, respectively. The notation $\mathcal{O}(g(x))$ denotes a quantity whose magnitude is bounded by a constant multiple of $|g(x)|$ in the stated limit, whereas $o(g(x))$ denotes a quantity whose ratio to $g(x)$ tends to zero in that limit.

2. System Model

As shown in Figure 1, we consider a point-to-point mmWave link in which a transmitter equipped with a single RF chain serves a single-antenna receiver using either an N-element AG beamforming array or a dielectric lens with N selectable feeds. In the ideal AG reference, the RF chain drives all N antenna elements with equal-magnitude weights, while an independently adjustable phase shifter at each element controls the beam direction [7]. In the lens-enabled architecture, an RF switch connects the RF chain to one selected feed. The passive lens maps feed positions to beam directions, enabling beam steering through feed selection without per-element phase shifters. Both architectures operate under the same total transmit-power budget.

2.1. AG Beamforming and Lens-Enabled Beamforming

When each antenna is equipped with its own phase shifter, the transmitter can carry out the AG beamforming operation toward the intended user, as illustrated in Fig. 1 (right). Let $\mathbf{f}_{\mathrm{AG}} \in \mathbb{C}^{N\times 1}$ denote the AG beamformer under a constant-modulus (equal-gain) constraint, i.e., each entry has magnitude $1/\sqrt{N}$. Specifically,

$$\mathbf{f}_{\mathrm{AG}} = \frac{1}{\sqrt{N}}\left[\exp(\jmath\psi_1), \exp(\jmath\psi_2), \cdots, \exp(\jmath\psi_N)\right]^T, \quad (1)$$

where ψ_n is the phase shift applied at the n-th antenna.

Let $s \in \mathbb{C}$ with $\mathbb{E}\{|s|^2\} = 1$ denote the transmit symbol. The received baseband signal at the user is

$$y = \sqrt{P_t}\mathbf{h}^T\mathbf{f}_{\mathrm{AG}}s + w, \quad (2)$$

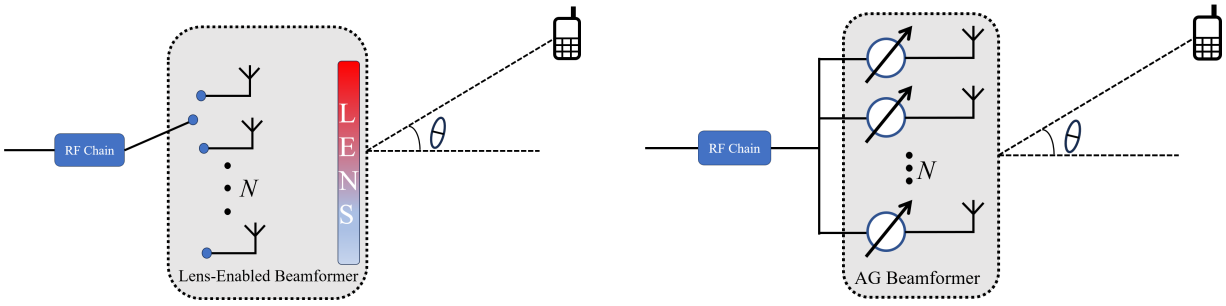


Figure 1: Lens-enabled transmitter with N feeds connected to a single RF chain (left) and the ideal AG phase-shifter reference (right).

where P_t is the total transmit power, $\mathbf{h} = [h^{(1)}, \cdots, h^{(N)}]^T \in \mathbb{C}^{N\times 1}$ is the channel vector to the user, and $w \sim \mathcal{CN}(0, N_0)$ models additive white Gaussian noise (AWGN) with noise power N_0. We define the transmit SNR as $\rho \triangleq P_t/N_0$. For typical far-field line-of-sight (LoS) propagation at mmWave, the channel vector can be modeled as [7, Eq. (3)][1]

$$\mathbf{h} = \alpha \mathbf{a}_\theta \tag{3}$$

where α is the complex path gain, θ is the angle-of-departure (AoD) to the user, and $\mathbf{a}_\theta \in \mathbb{C}^{N\times 1}$ with each element having unit magnitude is the array steering vector determined by the array geometry. For a half-wavelength spaced uniform linear array (ULA), $\mathbf{a}_\theta$ is of the form

$$\mathbf{a}_\theta = \left[1, \exp(\jmath\pi \sin(\theta)), \cdots, \exp(\jmath(N-1)\pi \sin(\theta))\right]^T. \tag{4}$$

The instantaneous SNR under AG beamforming is

$$\mathrm{SNR}_{\mathrm{AG}} = \rho \left|\mathbf{h}^T \mathbf{f}_{\mathrm{AG}}\right|^2. \tag{5}$$

Using $\mathbf{h} = \alpha \mathbf{a}_\theta$, we obtain

$$\left|\mathbf{h}^T \mathbf{f}_{\mathrm{AG}}\right|^2 = |\alpha|^2 \left|\mathbf{a}_\theta^T \mathbf{f}_{\mathrm{AG}}\right|^2 \overset{(a)}{\leq} |\alpha|^2 \|\mathbf{a}_\theta\|^2 = |\alpha|^2 N, \tag{6}$$

where (a) follows from the Cauchy–Schwarz inequality. Equality holds when the beamformer aligns with the array response. Thus, the optimal AG beamformer takes the form

$$\mathbf{f}_{\mathrm{AG}}^\star = \frac{1}{\sqrt{N}} \mathbf{a}_\theta^*. \tag{7}$$

The optimal SNR then takes the form

$$\mathrm{SNR}_{\mathrm{AG}} = \rho N |\alpha|^2. \tag{8}$$

Equation (8) uses the normalized isotropic-element reference adopted throughout the numerical comparison. If a realized element/scan power pattern $g_{\mathrm{e}}(\theta)$ is available, the same derivation gives $\mathrm{SNR}_{\mathrm{AG}} = \rho N g_{\mathrm{e}}(\theta)|\alpha|^2$. Hence the corresponding AoD-dependent loss can be incorporated by replacing N with $N g_{\mathrm{e}}(\theta)$. The ideal isotropic-element reference used here sets $g_{\mathrm{e}}(\theta) = 1$. Its beam is aligned separately to each intended AoD, assumed known at the transmitter. Compared with a single-antenna transmitter ($\mathrm{SNR} = \rho|\alpha|^2$), the array gain of the optimal AG beamformer is

$$G_{\mathrm{AG}} = \frac{\mathbb{E}\{\rho N |\alpha|^2\}}{\mathbb{E}\{\rho |\alpha|^2\}} = N. \tag{9}$$

Under the channel model (3), the optimal full-digital (FD) beamformer with N RF chains $\left(\mathbf{f}_{\mathrm{FD}}^\star = \mathbf{h}^*/\|\mathbf{h}\|\right)$ achieves the same SNR—and thus the same array gain N—as the optimal phase-only AG beamformer.

As shown in Fig. 1 (left), we adopt a feed-selection strategy in which the active feed is chosen to maximize the realized directional gain toward the intended AoD. Under the common-scalar channel model in (3), this is also the feed that maximizes the instantaneous received SNR. Specifically, letting $[N] \triangleq \{1, 2, \ldots, N\}$ and denoting by $G_\theta^{(n)}$ the complex field-gain coefficient when the n-th feed is active toward AoD θ, with power gain $g_\theta^{(n)} \triangleq |G_\theta^{(n)}|^2$, we select

$$n^\star = \arg\max_{n\in[N]} \left|G_\theta^{(n)} h^{(n)}\right|^2 = \arg\max_{n\in[N]} g_\theta^{(n)}, \tag{10}$$

where the simplification in the second equality follows from $\mathbf{h} = \alpha \mathbf{a}_\theta$: one has $|G_\theta^{(n)} h^{(n)}|^2 = g_\theta^{(n)}|\alpha|^2$, and the common random factor $|\alpha|^2$ does not affect the maximizing feed index.

Under the selection policy in (10), the received SNR is

$$\mathrm{SNR}_{\mathrm{Len}} = \rho |G_\theta^{(n^\star)} h^{(n^\star)}|^2 = \rho g_\theta^{(n^\star)} |\alpha|^2. \tag{11}$$

Hence, relative to a single-antenna transmitter ($\mathrm{SNR} = \rho|\alpha|^2$), the lens-enabled array gain is

$$G_{\mathrm{Len}} = \frac{\mathbb{E}\{\rho |G_\theta^{(n^\star)}|^2 |\alpha|^2\}}{\mathbb{E}\{\rho |\alpha|^2\}} = |G_\theta^{(n^\star)}|^2. \tag{12}$$

2.2. Independently Fluctuating Two-Ray (IFTR) Fading Channel

In the IFTR model, the small-scale fading is dominated by two strong specular waves superimposed on a diffuse

[1] Equation (3) is a single-dominant-path far-field model: the common scalar α captures the small-scale path fluctuation, while the deterministic steering vector captures the element-dependent phases. This model is consistent with the LoS-dominant mmWave setting considered here [7, 22].

background. Specializing the complex path gain α in (3) to this two-ray structure, we write [15]

$$\alpha = \sqrt{\xi_1} V_1 \exp(\jmath\phi_1) + \sqrt{\xi_2} V_2 \exp(\jmath\phi_2) + Z, \tag{13}$$

where $V_i \exp(\jmath\phi_i)$ is the i-th specular component for $i \in \{1, 2\}$, the phases ϕ_1 and ϕ_2 are independent and uniformly distributed over $[0, 2\pi)$, and $Z \sim \mathcal{CN}(0, 2\sigma^2)$ captures the aggregate diffuse term. The factors ξ_1 and ξ_2 model independent random fluctuations of the two specular amplitudes. They are also independent of the phases and of Z. Each ξ_i is unit-mean Gamma distributed with probability density function (PDF)

$$f_{\xi_i}(u) = \frac{m_i^{m_i} u^{m_i - 1}}{\Gamma(m_i)} \exp(-m_i u), \tag{14}$$

where $m_i > 0$ is the shape parameter, and $\Gamma(\cdot)$ denotes the Gamma function [23].

The IFTR model does not require an ordering of the specular amplitudes. We label the larger-amplitude component as component 1, so that $V_1 \geq V_2$, and associate m_1 with its fluctuation. Exchanging the pairs (V_1, m_1) and (V_2, m_2) leaves the channel distribution unchanged. Under this indexing convention, define [15]

$$K \triangleq \frac{V_1^2 + V_2^2}{2\sigma^2}, \; K_1 \triangleq \frac{V_1^2}{2\sigma^2}, \; K_2 \triangleq \frac{V_2^2}{2\sigma^2}, \tag{15}$$

$$\Delta \triangleq \frac{2V_1 V_2}{V_1^2 + V_2^2}. \tag{16}$$

Here, K is the ratio of the average specular power to the diffuse power, while $\Delta \in [0, 1]$ measures the relative balance of the two specular components. In particular, $\Delta = 1$ corresponds to equal specular amplitudes. If one specular component vanishes, $\Delta = 0$ and the IFTR model reduces to a single fluctuating-specular-wave model. Ordinary Rician fading is recovered when the remaining specular amplitude becomes nonfluctuating (equivalently, in the limit of an infinite Gamma shape parameter). Based on (13), the average channel power is

$$\mathbb{E}\{|\alpha|^2\} = V_1^2 + V_2^2 + 2\sigma^2 = 2\sigma^2(K + 1). \tag{17}$$

To normalize the channel power, we set $\sigma^2 = \frac{1}{2(K+1)}$. This normalization sets the average channel power to unity, i.e., $\mathbb{E}\{|\alpha|^2\} = 1$, and will be used throughout the analysis.

3. Asymptotic ETR Analysis and Threshold Optimization

Fixed-rate transmission is in outage whenever the instantaneous SNR falls below the decoding threshold. ETR accounts for these unsuccessful transmissions by weighting the fixed spectral efficiency by the probability of successful decoding. We derive a common threshold rule for the AG and lens-enabled links, whose deterministic gains enter through the average SNR.

We consider transmission at the fixed spectral efficiency $\log_2(1 + \gamma_{th})$ bit/s/Hz, where γ_{th} is the minimum SNR required for successful decoding at the user. The OP is defined as $P_{\text{out}}(\gamma_{th}) \triangleq \Pr\{\text{SNR} \leq \gamma_{th}\}$. The ETR is therefore defined as [24, 25]

$$R \triangleq \big(1 - P_{\text{out}}(\gamma_{th})\big) \log_2(1 + \gamma_{th}). \tag{18}$$

We begin by introducing the scalar

$$A_0 \triangleq \frac{m_1^{m_1} m_2^{m_2}}{(K_1 + m_1)^{m_1} (K_2 + m_2)^{m_2}} \times {}_2F_1\left(m_1, m_2; 1; \frac{K^2 \Delta^2}{4(K_1 + m_1)(K_2 + m_2)}\right), \tag{19}$$

where ${}_2F_1(\cdot, \cdot; \cdot; \cdot)$ is the Gauss hypergeometric function [23]. With this notation, both architectures can be treated through the same deterministic received-SNR scale. Let $\bar{\gamma}$ denote the average received SNR after beamforming. Considering the SNR expressions for AG beamforming and lens-enabled beam selection in (8) and (11), respectively, together with $\mathbb{E}\{|\alpha|^2\} = 1$, we obtain $\bar{\gamma} = \rho N$ for AG beamforming and $\bar{\gamma} = \rho g_\theta^{(n^\star)}$ for lens-enabled beam selection. The common rate-design rule is stated next.

Lemma 1. *For an IFTR link with instantaneous SNR $\gamma = \bar{\gamma}|\alpha|^2$, the high-SNR asymptotic OP can be expressed as*

$$P_{\text{out}}(\gamma_{th}) \simeq \Theta \gamma_{th}, \tag{20}$$

where

$$\Theta \triangleq \frac{A_0(1 + K)}{\bar{\gamma}}. \tag{21}$$

By substituting this asymptotic OP into the ETR, the resulting approximate ETR is uniquely maximized at

$$\gamma_{th,\text{asy}}^\star = \frac{1 + \Theta}{\Theta W\left(\frac{e(1+\Theta)}{\Theta}\right)} - 1, \tag{22}$$

where $W(\cdot)$ denotes the principal branch of the Lambert W function [23]. As $\Theta \to 0$, the above threshold admits the leading-order approximation

$$\gamma_{th,\text{asy}}^\star \simeq \frac{1}{\Theta(1 - \ln \Theta)}. \tag{23}$$

For the two architectures considered in this work, the parameter Θ specializes to $\Theta_{\text{AG}} = A_0(1 + K)/(\rho N)$ for AG beamforming and $\Theta_{\text{Len}} = A_0(1 + K)/(\rho g_\theta^{(n^\star)})$ for lens-enabled beamforming.

Proof. The proof is given in Appendix A. ∎

For a given $\bar{\gamma}$, both architectures have the same OP and ETR under the common scalar IFTR model. Their system-level difference therefore comes from the directional gain, not from different fading statistics.

Remark 1. *The measurement fit for the far-field outdoor scenario at 28 GHz in [20, Table II] gives $K = 467.5652$ in the IFTR channel model. For a given decoding threshold and average received SNR, such a large K increases the normalized argument $z = (1+K)\gamma_{th}/\bar{\gamma}$, so the small-$z$ condition underlying the high-SNR OP approximation may not hold at practical SNRs. Consequently, the approximation can be highly inaccurate in this regime.*

The high-SNR OP approximation is derived for a fixed decoding threshold as the average received SNR $\bar{\gamma}$ increases. In ETR optimization, however, the designed threshold also changes with $\bar{\gamma}$. To apply the approximation at this varying threshold, we must verify that the normalized argument $z = (1+K)\gamma_{th}/\bar{\gamma}$ still tends to zero. Remark 2 establishes this limiting behavior, while Section 5 quantifies the ETR loss at finite SNRs.

Remark 2 (Moving threshold at high SNR)**.** *For fixed IFTR channel parameters, write $\Theta = c_0/\bar{\gamma}$, where $c_0 = A_0(1+K) > 0$ is constant. The closed-form threshold in (23) then satisfies $\gamma^{\star}_{th,\mathrm{asy}} = \mathcal{O}(\bar{\gamma}/\ln\bar{\gamma})$. Its normalized argument therefore satisfies $z = (1+K)\gamma^{\star}_{th,\mathrm{asy}}/\bar{\gamma} = \mathcal{O}(1/\ln\bar{\gamma}) \to 0$ as $\bar{\gamma} \to \infty$. Thus, the designed threshold grows more slowly than the average received SNR, and the small-z condition required by the OP expansion remains satisfied asymptotically. However, this logarithmic convergence does not guarantee accuracy at practical SNRs. Section 4 provides the exact ETR benchmark used to assess the resulting design loss.*

4. Exact IFTR Benchmark and Accuracy of the Asymptotic Rate Design

We now use the exact IFTR Gamma mixture [20] to derive an ETR stationary condition and quantify the error of the asymptotic threshold rule.

4.1. Exact ETR Characterization

For either architecture, let $\bar{\gamma} = \rho N$ for the AG reference or $\bar{\gamma} = \rho g_{\theta}^{(n^{\star})}$ for lens-enabled beam selection, as in Section 3. Set

$$z \triangleq \frac{(1+K)\gamma_{th}}{\bar{\gamma}}. \tag{24}$$

Set $c = (1+K)/\bar{\gamma}$. The exact PDF of the instantaneous SNR γ over IFTR fading channels is of the form [20]

$$f_{\gamma}(x) = c\exp(-cx)\sum_{j=0}^{\infty} A_j \frac{(cx)^j}{j!}, \qquad x \geq 0. \tag{25}$$

Define $a_i = m_i + K_i$ and $q = K_1K_2/(a_1a_2)$. Equivalently, $q = K^2\Delta^2/(4a_1a_2)$. The complete mixture coefficients are [20, Eq. (11)]

$$\begin{aligned} A_j = {} & \frac{m_1^{m_1}m_2^{m_2}}{j!\Gamma(m_1)\Gamma(m_2)} \sum_{k=0}^{j}\binom{j}{k}\sum_{v=0}^{j-k}\binom{j-k}{v}K_1^{v}K_2^{j-k-v} \\ & \times \sum_{\ell=0}^{k}\binom{k}{\ell}(-1)^k(K_1K_2)^{\ell}\frac{\Gamma(m_1+v+\ell)}{a_1^{m_1+v+\ell}} \\ & \times \frac{\Gamma(m_2+j-k-v+\ell)}{a_2^{m_2+j-k-v+\ell}} \\ & \times {}_2\widetilde{F}_1\left(\begin{matrix} m_1+v+\ell,\ m_2+j-k-v+\ell \\ 2\ell-k+1 \end{matrix}; q\right). \end{aligned} \tag{26}$$

Here ${}_2\widetilde{F}_1(a,b;d;q) = \sum_{n=0}^{\infty}(a)_n(b)_n q^n/[\Gamma(d+n)n!]$ is the regularized Gauss hypergeometric function, and $(a)_n$ is the Pochhammer symbol. When $d+n$ is a nonpositive integer, the corresponding series term is zero because $1/\Gamma(d+n) = 0$. The series therefore remains well defined for nonpositive integer d, for which the relation ${}_2\widetilde{F}_1(a,b;d;q) = {}_2F_1(a,b;d;q)/\Gamma(d)$ must be understood through a limit rather than direct substitution [20]. The coefficients satisfy $A_j \geq 0$ and $\sum_j A_j = 1$.

The $j = 0$ case is already given in (19). To state the $j = 1$ case explicitly, set $C = m_1^{m_1}m_2^{m_2}/(a_1^{m_1}a_2^{m_2})$, $B = m_1K_1/a_1 + m_2K_2/a_2$, and $D = 2 - K_1/a_1 - K_2/a_2$. Then

$$\begin{aligned} A_1 = C\big[& B\,{}_2F_1(m_1,m_2;1;q) \\ & - qDm_1m_2\,{}_2F_1(m_1+1,m_2+1;2;q)\big]. \end{aligned} \tag{27}$$

The probability-generating function $G(t) = \sum_{j=0}^{\infty}A_jt^j$ provides a direct check of the coefficients. The index j is the nonnegative integer indexing the Gamma-mixture components. This series converges absolutely for $|t| \leq 1$, since the weights sum to one. With $u = 1-t$, it is

$$\begin{aligned} G(t) = {} & \left(\frac{m_1}{m_1+K_1u}\right)^{m_1}\left(\frac{m_2}{m_2+K_2u}\right)^{m_2} \\ & \times {}_2F_1\left(m_1,m_2;1;\frac{K_1K_2u^2}{(m_1+K_1u)(m_2+K_2u)}\right). \end{aligned} \tag{28}$$

To obtain (28), average $\exp[-(1-t)S]$ with $S = K_1\xi_1 + K_2\xi_2 + 2\sqrt{K_1K_2\xi_1\xi_2}\cos\phi$, where ξ_i are the unit-mean Gamma variables in (13) and $\phi = \phi_1 - \phi_2$ is uniform modulo 2π. Conditional on S, the weights are Poisson probabilities, $A_j = \mathbb{E}\{\exp(-S)S^j/j!\}$. Differentiation at $t = 0$ gives $A_0 = G(0)$ and $A_1 = G'(0)$, yielding (19) and (27).

Based on the PDF in (25), the exact cumulative distribution function (CDF) can be expressed as

$$F_{\gamma}(\gamma_{th}) = \sum_{j=0}^{\infty}A_j\left[1 - \exp(-z)\sum_{k=0}^{j}\frac{z^k}{k!}\right], \tag{29}$$

Hence, the corresponding complementary cumulative distribution function (CCDF) is

$$\bar{F}_{\gamma}(\gamma_{th}) = \exp(-z)\sum_{j=0}^{\infty}A_j\sum_{k=0}^{j}\frac{z^k}{k!}. \tag{30}$$

The exact ETR is therefore

$$R_{\mathrm{ex}}(\gamma_{th}) = \bar{F}_{\gamma}(\gamma_{th})\log_2(1+\gamma_{th}). \tag{31}$$

The IFTR PDF is analytic: $0 \le A_j \le 1$ ensures compact-uniform convergence of $\sum_j A_j z^j/j!$ and its differentiated series. Termwise differentiation is therefore valid on every finite interval. Since $F'_\gamma(x) = f_\gamma(x)$, the CDF is continuously differentiable to every order for $x > 0$. Multiplication by $\log_2(1+x)$ then gives the same regularity for $R_{\rm ex}(x)$, including the second derivative used in Proposition 3.

Proposition 1. *Let $\gamma^\star_{th,\rm ex}$ denote a global maximizer of the exact ETR in (31). This maximizer is interior and positive, and satisfies*

$$(1+\gamma^\star_{th,\rm ex})\ln(1+\gamma^\star_{th,\rm ex}) f_\gamma(\gamma^\star_{th,\rm ex}) = \bar{F}_\gamma(\gamma^\star_{th,\rm ex}), \quad (32)$$

where $f_\gamma(\cdot)$ and $\bar{F}_\gamma(\cdot)$ denote the exact IFTR SNR PDF and CCDF, respectively. Defining the hazard function associated with the exact IFTR SNR distribution as

$$\mathcal{H}_\gamma(x) \triangleq \frac{f_\gamma(x)}{\bar{F}_\gamma(x)}, \quad (33)$$

the stationary condition can equivalently be expressed as

$$\mathcal{H}_\gamma(\gamma^\star_{th,\rm ex}) = \frac{1}{(1+\gamma^\star_{th,\rm ex})\ln(1+\gamma^\star_{th,\rm ex})}. \quad (34)$$

Any stationary threshold $x_0 > 0$ is a strict local maximizer if the first derivative of $\mathcal{H}_\gamma(x_0)$ satisfies

$$\mathcal{H}'_\gamma(x_0) > -\frac{\ln(1+x_0)+1}{(1+x_0)^2\ln^2(1+x_0)}. \quad (35)$$

If (35) holds for every $x_0 > 0$, the exact ETR has a unique stationary point, which is its unique global maximizer.

Proof. Since $\mathbb{E}\{\gamma\} = \bar{\gamma}$, Markov's inequality gives

$$R_{\rm ex}(x) \le \frac{\bar{\gamma}}{x}\log_2(1+x) \to 0 \quad \text{as } x \to \infty. \quad (36)$$

Choose any $x_1 > 0$. Because $R_{\rm ex}(x_1) > 0$ and $R_{\rm ex}(x) \to 0$ as $x \to \infty$, there is an $M > x_1$ such that $R_{\rm ex}(x) < R_{\rm ex}(x_1)$ for all $x \ge M$. Continuity guarantees a maximum on the compact interval $[0, M]$. Neither endpoint can attain it, so at least one global maximizer lies in $(0, M)$. This existence argument permits multiple stationary points or maximizers. Uniqueness requires the additional condition stated in the proposition.

Differentiating (31) with respect to γ_{th} gives

$$\frac{{\rm d}R_{\rm ex}}{{\rm d}\gamma_{th}} = -f_\gamma(\gamma_{th})\log_2(1+\gamma_{th}) + \frac{\bar{F}_\gamma(\gamma_{th})}{(1+\gamma_{th})\ln 2}. \quad (37)$$

Using (33), this derivative can be written as

$$\frac{{\rm d}R_{\rm ex}}{{\rm d}\gamma_{th}} = \frac{\bar{F}_\gamma(\gamma_{th})\ln(1+\gamma_{th})}{\ln 2}\Psi(\gamma_{th}), \quad (38)$$

where

$$\Psi(x) \triangleq \frac{1}{(1+x)\ln(1+x)} - \mathcal{H}_\gamma(x). \quad (39)$$

For $x > 0$, $\bar{F}_\gamma(x) \ge A_0\exp(-cx) > 0$ because $A_0 = \mathbb{E}\{\exp(-S)\} > 0$. Also $\ln(1+x) > 0$ and $\ln 2 > 0$. Thus the factor preceding $\Psi(\gamma_{th})$ in (38) is strictly positive, and any interior stationary point satisfies $\Psi(\gamma_{th}) = 0$, which gives (32) and (34).

Differentiating (39) yields

$$\Psi'(x) = -\frac{\ln(1+x)+1}{(1+x)^2\ln^2(1+x)} - \mathcal{H}'_\gamma(x). \quad (40)$$

Therefore, (35) implies $\Psi'(x_0) < 0$. The derivative of the ETR then changes locally from positive to negative, establishing a strict local maximum.

If (35) holds for every $x_0 > 0$, then $\Psi'(x) < 0$ for all $x > 0$. The function Ψ is strictly decreasing and has a zero at the interior maximizer whose existence was just proved. It therefore has exactly one zero, so the ETR has a unique stationary point and global maximizer. ■

The condition on the hazard derivative guarantees a unique ETR maximizer, but it need not hold for every IFTR channel. The numerical benchmark therefore does not assume uniqueness: it evaluates the exact ETR at all candidate maxima and selects the one with the largest value.

4.2. Second-Order High-SNR Expansion

The high-SNR asymptotic OP used in Lemma 1 retains the leading term of the IFTR CDF. The Gamma-mixture representation further permits a second-order characterization as the normalized argument z approaches zero.

Proposition 2. *For fixed IFTR parameters and $z \to 0$, the exact OP over IFTR channels admits the expansion*

$$F_\gamma(\gamma_{th}) = A_0 z + \frac{A_1 - A_0}{2}z^2 + \mathcal{O}(z^3), \quad (41)$$

where A_0 and A_1 are given by (19) and (27) respectively.

Proof. From (29), the $j = 0$ Gamma component satisfies

$$1 - \exp(-z) = z - \frac{z^2}{2} + \mathcal{O}(z^3), \quad (42)$$

whereas the $j = 1$ component satisfies

$$1 - \exp(-z)(1+z) = \frac{z^2}{2} + \mathcal{O}(z^3). \quad (43)$$

For the remaining components, let $P(a, z)$ denote the regularized lower incomplete Gamma function, defined by

$$P(a,z) = \frac{1}{\Gamma(a)}\int_0^z t^{a-1}\exp(-t)\,{\rm d}t. \quad (44)$$

This definition distinguishes P from the unregularized lower incomplete Gamma function. Since $P(j+1, z)$ is nonincreasing in the integer shape parameter $j+1$ for fixed $z \ge 0$, and since $A_j \ge 0$ with $\sum_{j=0}^\infty A_j = 1$, their aggregate contribution satisfies

$$0 \le \sum_{j=2}^\infty A_j P(j+1, z) \le P(3, z)\sum_{j=2}^\infty A_j$$

$$\leq P(3, z) = \mathcal{O}(z^3). \tag{45}$$

Hence, the entire infinite tail contributes only at order z^3 or higher. Collecting the first- and second-order terms gives (41), which completes the proof. ■

Proposition 2 identifies the first correction to the high-SNR OP approximation in (20), where $\Theta\gamma_{th} = A_0 z$. The second-order correction is $(A_1 - A_0)z^2/2$: it combines the contribution $-A_0 z^2/2$ from the $j = 0$ component with $A_1 z^2/2$ from the $j = 1$ component and therefore cannot be obtained by expanding the $j = 0$ component alone. For fixed channel parameters and a fixed threshold, z decreases proportionally to $\bar{\gamma}^{-1}$, so this correction is $\mathcal{O}(\bar{\gamma}^{-2})$. At the SNR-dependent threshold in (22), Remark 2 instead gives $z = \mathcal{O}(1/\ln\bar{\gamma}) \to 0$, with a second-order correction of $\mathcal{O}(1/(\ln\bar{\gamma})^2)$. The OP expansion thus remains applicable asymptotically. But, its asymptotic validity alone does not establish the ETR design accuracy at practical SNRs, which is assessed separately using the exact ETR benchmark.

4.3. Threshold Error and ETR Loss

A threshold approximation can deviate noticeably from the exact maximizer while still providing an ETR close to the optimum. To characterize this effect, recall the exact ETR-maximizing threshold $\gamma^\star_{th,\mathrm{ex}}$ defined in Proposition 1, and let $\widehat{\gamma}_{th}$ denote an approximate threshold obtained from a low-complexity design rule. Define the relative threshold error as

$$\epsilon_\gamma \triangleq \frac{|\widehat{\gamma}_{th} - \gamma^\star_{th,\mathrm{ex}}|}{\gamma^\star_{th,\mathrm{ex}}}, \tag{46}$$

and the relative ETR loss as

$$\epsilon_R^{\mathrm{loc}} \triangleq 1 - \frac{R_{\mathrm{ex}}(\widehat{\gamma}_{th})}{R_{\mathrm{ex}}(\gamma^\star_{th,\mathrm{ex}})}. \tag{47}$$

The denominator is the largest ETR attainable on this same physical channel. Thus $\epsilon_R^{\mathrm{loc}}$ is the fraction of optimal ETR lost by using the perturbed threshold. It is dimensionless and belongs to $[0, 1]$ for every nonnegative threshold. The superscript loc distinguishes the threshold-perturbation analysis from the surrogate-design loss introduced in Section 5.1.

Write $R'_{\mathrm{ex}}(x) = \mathrm{d}R_{\mathrm{ex}}(x)/\mathrm{d}x$ and $R''_{\mathrm{ex}}(x) = \mathrm{d}^2 R_{\mathrm{ex}}(x)/\mathrm{d}x^2$ for the first and second derivatives with respect to the decoding threshold. Their existence follows from the Gamma-mixture regularity established in Section 4.1.

Proposition 3. *For an interior maximizer $\gamma^\star_{th,\mathrm{ex}}$, suppose that $R''_{\mathrm{ex}}(\gamma^\star_{th,\mathrm{ex}}) < 0$. For $\widehat{\gamma}_{th} = \gamma^\star_{th,\mathrm{ex}} + \Delta\gamma$ with $\Delta\gamma \to 0$, the relative ETR loss satisfies*

$$\epsilon_R^{\mathrm{loc}} = \frac{\kappa^{\mathrm{ex}}}{2}\left(\frac{\Delta\gamma}{\gamma^\star_{th,\mathrm{ex}}}\right)^2 + o\left(\left(\frac{\Delta\gamma}{\gamma^\star_{th,\mathrm{ex}}}\right)^2\right), \tag{48}$$

where

$$\kappa^{\mathrm{ex}} \triangleq -\frac{(\gamma^\star_{th,\mathrm{ex}})^2 R''_{\mathrm{ex}}(\gamma^\star_{th,\mathrm{ex}})}{R_{\mathrm{ex}}(\gamma^\star_{th,\mathrm{ex}})} > 0 \tag{49}$$

Table 1
Numerical verification of Proposition 3 for the fitted physical IFTR channel at $\bar{\gamma} = 10$ dB.

δ (%)	Exact loss $\epsilon_R^{\mathrm{loc}}$ (%)	Quadratic loss $\frac{\kappa^{\mathrm{ex}}}{2}\delta^2$ (%)	Relative difference (%)
-5	0.0718874	0.0702791	2.24
-1	0.0028235	0.0028112	0.44
+1	0.0027991	0.0028112	0.43
+5	0.0688303	0.0702791	2.10

Relative difference is the absolute difference between the quadratic and exact losses, divided by the exact loss.

is a dimensionless measure of the sharpness of the ETR peak.

Proof. A second-order Taylor expansion around $\gamma^\star_{th,\mathrm{ex}}$ gives

$$R_{\mathrm{ex}}(\widehat{\gamma}_{th}) = R_{\mathrm{ex}}(\gamma^\star_{th,\mathrm{ex}}) + R'_{\mathrm{ex}}(\gamma^\star_{th,\mathrm{ex}})\Delta\gamma + \frac{1}{2}R''_{\mathrm{ex}}(\gamma^\star_{th,\mathrm{ex}})(\Delta\gamma)^2 + o((\Delta\gamma)^2). \tag{50}$$

Since $R'_{\mathrm{ex}}(\gamma^\star_{th,\mathrm{ex}}) = 0$, substituting this expansion into (47) and using (49) yields (48). ■

Proposition 3 shows that, near the exact optimum, the relative ETR loss is approximately $\kappa^{\mathrm{ex}}/2$ times the squared relative threshold error. Thus, doubling a sufficiently small relative threshold error approximately quadruples the ETR loss. The coefficient κ^{ex} measures the sensitivity of ETR to this error: a larger value indicates a sharper peak and greater loss, whereas a smaller value indicates a flatter peak and greater tolerance to threshold errors. Consequently, a threshold error need not imply a comparable ETR loss. For larger deviations, the local expansion in (48) does not guarantee accuracy, and the ETR loss is evaluated directly using the exact benchmark in (31). We therefore report both the relative threshold error in (46) and the relative ETR loss in (47) when assessing the asymptotic design.

For the IFTR channel fitted to the far-field outdoor measurements at 28 GHz in [20, Table II][2], at an average received SNR of $\bar{\gamma} = 10$ dB, the exact-mixture calculation gives $\gamma^\star_{th,\mathrm{ex}} = 6.14579$ and $\kappa^{\mathrm{ex}} = 0.562233$. Table 1 compares the exact loss with (48), using $\delta = \Delta\gamma/\gamma^\star_{th,\mathrm{ex}}$. The quadratic dependence predicts a 25-fold reduction in loss when $|\delta|$ decreases from 5% to 1%. The exact reductions are 25.46-fold and 24.59-fold for negative and positive perturbations, respectively. The relative discrepancy also falls from 2.10–2.24% to 0.43–0.44%. Thus the loss follows the predicted square dependence more closely as the perturbation shrinks, consistent with the $o(\delta^2)$ remainder.

5. Numerical Results

We first assess threshold-design accuracy and physical-channel sensitivity. We then combine the statistical model with the full-wave lens radiation patterns to compare the two transmitter architectures.

[2] The fitted IFTR parameters are $K = 467.5652$, $\Delta = 0.8487$, $m_1 = 9.2$, and $m_2 = 50.6$.

5.1. Surrogate Threshold Design and Physical-Channel Sensitivity

Motivated by the finite-SNR limitation identified in Remark 1, we introduce a design-surrogate parameter K_s solely for computing the asymptotic threshold. The physical channel model remains unchanged. For a given K_s, the corresponding specular ratios are reconstructed using the physical value of Δ as

$$K_{1,s} = \frac{K_s}{2}\left(1+\sqrt{1-\Delta^2}\right),$$
$$K_{2,s} = \frac{K_s}{2}\left(1-\sqrt{1-\Delta^2}\right), \tag{51}$$

where $K_{1,s} \geq K_{2,s}$ preserves the component labeling of the fitted channel, so that m_1 and m_2 remain associated with the same specular components. The coefficient $A_{0,s}$ is obtained from (19) by replacing (K, K_1, K_2) with $(K_s, K_{1,s}, K_{2,s})$, yielding $\Theta_s = A_{0,s}(1+K_s)/\bar{\gamma}$. The resulting threshold, denoted by $\widehat{\gamma}_{th}(K_s)$, is then obtained from Lemma 1. Importantly, K_s enters only this low-complexity design rule. In each test, all performance metrics are evaluated on the specified physical IFTR channel; K_s is used only for threshold design.

Specifically, write $\mathbf{p} = (K, \Delta, m_1, m_2, \bar{\gamma})$ for the physical channel parameters, and define the physical-channel loss of the surrogate design by

$$\epsilon_R^{\mathrm{sur}}(K_s;\mathbf{p}) = 1 - \frac{R_{\mathrm{ex}}(\widehat{\gamma}_{th}(K_s);\mathbf{p})}{R_{\mathrm{ex}}(\gamma^{\star}_{th,\mathrm{ex}}(\mathbf{p});\mathbf{p})}. \tag{52}$$

Both ETR values are evaluated on the same physical IFTR channel with parameters $\mathbf{p}$ and the same average received SNR; K_s is used only to design the threshold $\widehat{\gamma}_{th}(K_s)$. Since the exact ETR is nonnegative and $\gamma^{\star}_{th,\mathrm{ex}}(\mathbf{p})$ is a global maximizer, we have

$$0 \leq R_{\mathrm{ex}}(\widehat{\gamma}_{th}(K_s);\mathbf{p}) \leq R_{\mathrm{ex}}(\gamma^{\star}_{th,\mathrm{ex}}(\mathbf{p});\mathbf{p}). \tag{53}$$

The maximum ETR in the denominator is positive, so $0 \leq \epsilon_R^{\mathrm{sur}}(K_s;\mathbf{p}) \leq 1$, even when $K_s \neq K$. This bound would not generally hold for a ratio evaluated on two different physical channels. When $\mathbf{p}$ is fixed, we omit it from the notation for brevity.[3]

To isolate the accuracy of the rate-design rule from the deterministic beamforming gain, we first evaluate (52) directly as a function of the average received SNR $\bar{\gamma}$, with the physical IFTR parameters fixed at $K = 467.5652$, $\Delta = 0.8487$, $m_1 = 9.2$, and $m_2 = 50.6$ for the channel measurements at 28 GHz.

For numerical evaluation, the CDF and CCDF sums are truncated at $j = J$. Let $F_{\gamma,J}$ and $\bar{F}_{\gamma,J}$ denote the corresponding partial sums, and set $r_J = \sum_{j>J} A_j$. Since each Gamma CDF and CCDF lies in $[0,1]$, we have

$$0 \leq F_{\gamma}(x) - F_{\gamma,J}(x) \leq r_J,$$

[3]The surrogate loss measures the ETR penalty incurred by using the threshold designed with K_s, whereas $\epsilon_R^{\mathrm{loc}}$ describes the loss caused by a small threshold perturbation around the exact optimum. The local expansion in (48) therefore approximates the surrogate loss only when the designed threshold is sufficiently close to the exact optimal threshold.

Table 2
Accuracy of the surrogate threshold design for the fitted IFTR channel.

$\bar{\gamma}$ (dB)	$\gamma^{\star}_{th,\mathrm{ex}}$	$\widehat{\gamma}_{th}(15)$	ϵ_{γ} (%)	$\epsilon_R^{\mathrm{sur}}(15)$ (%)	$\epsilon_R^{\mathrm{sur}}(467.5652)$ (%)
0	0.906	0.989	9.1	0.63	99.997
5	2.449	2.674	9.2	0.40	99.887
10	6.146	6.984	13.6	0.50	98.478
15	14.482	18.119	25.1	0.94	92.405
20	33.778	47.491	40.6	1.62	80.721
25	83.270	126.605	52.0	2.17	67.459
30	217.658	343.616	57.9	2.40	56.329

$$0 \leq \bar{F}_{\gamma}(x) - \bar{F}_{\gamma,J}(x) \leq r_J. \tag{54}$$

The ETR truncation error is at most $r_J \log_2(1+x)$. For $K > 0$, the nonnegative mixture coefficients provide a bound on the omitted probability mass. For any $t_0 > 1$ such that $G(t_0) < \infty$, we have $r_J t_0^{J+1} \leq \sum_{j=J+1}^{\infty} A_j t_0^j \leq G(t_0)$. We therefore obtain

$$r_J \leq \frac{G(t_0)}{t_0^{J+1}}. \tag{55}$$

We choose $t_0 = 1 + m_1 m_2/[2(m_1 K_2 + m_2 K_1)] > 1$. To verify that $G(t_0)$ is finite, let $\hbar = t_0 - 1$. Then $m_i - K_i\hbar > 0$ for $i = 1, 2$, and $(m_1 - K_1\hbar)(m_2 - K_2\hbar) - K_1K_2\hbar^2 = m_1m_2/2 > 0$. Hence, the hypergeometric argument in (28) lies in $[0, 1)$, ensuring that $G(t_0)$ is finite. For $K = 0$, only $A_0 = 1$ is nonzero, so no truncation is needed.

For the fitted IFTR channel, we compute t_0 and $G(t_0)$ and choose $J = 2954$, which makes the truncation bound in (55) smaller than 10^{-10}. The coefficients $A_0, \ldots, A_J$ are extracted from (28) by numerical Fourier inversion, with convergence checked by doubling the resolution.

Using these coefficients, we construct the truncated ETR objective. The bound in (36) excludes sufficiently large thresholds whose ETR upper bound falls below a value already attained, restricting the search to a finite interval. We locate and compare the candidate maxima within this interval to obtain the numerical optimum. Independent Monte Carlo channel simulations provide a further check of the ETR results. This procedure is used throughout Tables 2–4.

Table 2 reports the threshold error and ETR loss for the fitted physical channel. With $K_s = 15$, the ETR loss is below 2.5% at all seven tested SNRs, although the threshold error reaches 57.9% at 30 dB. These losses are evaluated directly from the exact mixture. The local expansion is not used for large threshold errors. Using the fitted $K = 467.5652$ directly in the asymptotic rule produces much larger losses.

We note that the surrogate changes the threshold-design coefficient, not the distribution used to evaluate performance. Its accuracy is therefore assessed through the resulting threshold and physical-channel ETR loss, rather than similarity between the surrogate and physical CDFs.

To examine the dependence on the surrogate choice, Table 3 reports $\epsilon_R^{\mathrm{sur}}(K_s)$ for several moderate values of K_s, while the physical IFTR channel remains unchanged.

Table 3
ETR-loss sensitivity to the design-surrogate parameter K_s. Losses are rounded to two decimal places.

$\bar{\gamma}$ (dB)	$K_s = 5$	$K_s = 10$	$K_s = 15$	$K_s = 20$	$K_s = 30$
	$\epsilon_R^{\mathrm{sur}}(K_s)$ (%)				
0	4.69	0.47	0.63	5.07	23.82
10	1.22	0.03	0.50	2.25	8.47
20	0.00	0.44	1.62	3.23	7.09
30	0.09	0.97	2.40	4.07	7.55

Among the values and SNRs in Table 3, $K_s = 10$ gives the smallest worst-case ETR loss (below 1%). We use $K_s = 15$ as a representative moderate surrogate in the system-level evaluation and Fig. 4. Table 3 shows that smaller losses can be obtained with other tested choices, so this representative value is not an optimized surrogate.

Table 4 varies one physical IFTR parameter at a time at $\bar{\gamma} = 10$ dB, with the others fixed at their fitted values. It reports the directly computed physical-channel optimum and the threshold error and physical-channel ETR loss for several K_s. In particular, the two Δ settings are scanned over $K_s \in \{0, 1, 2, 5, 10, 15, 20\}$. The case $K_s = 0$ is the Rayleigh-limit design reference.

Table 4 shows that, for $\Delta = 0.5$, reducing K_s from 15 to 2 lowers the threshold error from 1085.8% to 2.4% and the ETR loss from approximately 100% to 0.0302%, demonstrating that retuning can recover an accurate design in this setting. For $\Delta = 1$, retuning also improves performance: $K_s = 2$ reduces the threshold error to 48.0% and the ETR loss to 9.95%, compared with 63.2% and 20.08% for $K_s = 15$. However, this remains the smallest loss among the tested choices; $K_s = 0$ and 20 give losses of 11.79% and 22.07%, respectively. Here, $\Delta = 1$ corresponds to the boundary configuration with equal average powers in the two specular components, distinct from the fitted value $\Delta = 0.8487$. These results show that the moderate-K_s rule offers an accurate low-complexity design for the fitted channel and can accommodate some parameter changes through retuning, while exact ETR optimization is preferable for the balanced boundary case considered here.

5.2. Lens-Enabled Link Performance

We combine the IFTR channel model with the full-wave EM patterns validated against measurements of the fabricated dielectric lens illustrated in Fig. 2 [26]. The 160-mm lens has a 60-mm focal length and eight feed positions spaced by 7.2 mm, producing the patterns in Fig. 3 with a maximum boresight gain of approximately 28 dBi. The IFTR parameters are fixed to $K = 467.5652$, $\Delta = 0.8487$, $m_1 = 9.2$, and $m_2 = 50.6$ for channel measurements at 28 GHz [20, Table II].

Figure 4 shows the ETR versus fixed transmission spectral efficiency at $\rho = 0$ dB. For the measurement-fitted channel, the lens-enabled scheme achieves a higher maximum ETR than the AG reference[4] within approximately $|\theta| \leq 30°$, with a boresight ratio exceeding three. At $\theta = 35°$, the AG reference becomes superior as the realized lens gain decreases. The ETR achieved using the closed-form threshold in Lemma 1 agrees closely with the Monte Carlo maxima for the channel with $K = 15$, with all other IFTR parameters kept at their measurement-fitted values. Moreover, the threshold designed with $K_s = 15$ achieves an ETR close to the exact optimum on the measurement-fitted physical channel with $K = 467.5652$, with the resulting loss extensively quantified in Tables 2 and 3.

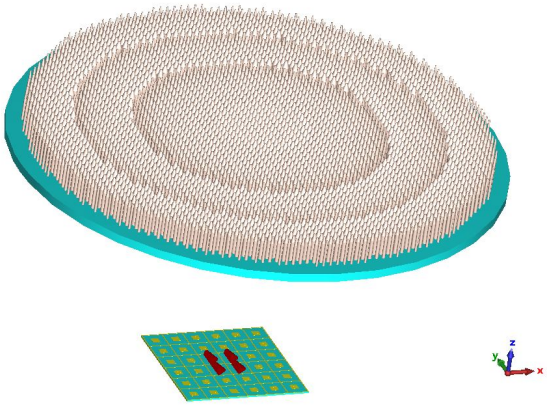


Figure 2: Full-wave EM simulation model of the dielectric lens in [26].

Remark 3 (Interpretation of the AG comparison)**.** *Figure 4 compares the lens-enabled architecture with the ideal AG reference using eight feeds or array elements, a single transmit RF chain, and the same total transmit power. The lens steers the beam through feed selection, whereas AG beamforming requires an independently adjustable phase shifter at each element. The comparison therefore evaluates the ETR attainable with these two beam-steering architectures under the stated gain models, while highlighting the lens architecture's reduced phase-control requirements. Since the physical apertures and EIRP are not matched, the observed ETR advantage applies to this equal-count, equal-power comparison rather than establishing superiority over an equal-aperture phased array.*

6. Conclusion

We studied ETR-maximizing threshold design for lens-enabled beam selection and an ideal single-RF-chain AG reference over IFTR fading. Under the common scalar channel model, the two architectures share the same rate-design objective at a given average received SNR. Their performance difference arises from the deterministic beamforming

[4]The ideal ULA radiation pattern follows analytically from its array factor. In the AG reference, however, the beamformer is adjusted to the intended AoD according to (7), rather than held at a fixed steering angle. The user therefore remains at the beam center, where the power gain is N for unit-magnitude isotropic-element responses and fixed total transmit power. Off-axis attenuation in a fixed-beam pattern does not apply to this aligned reference. Element-pattern and hardware losses are omitted from this ideal model, whereas the lens gain is taken from the supplied full-wave patterns.

Table 4
Physical-channel sensitivity at $\bar{\gamma} = 10$ dB. Each surrogate entry is $(\epsilon_\gamma, \epsilon_R^{\mathrm{sur}})$ in percent. Both ETR terms use the indicated physical channel. Losses are rounded to two decimal places.

Physical setting	$\gamma_{th,\mathrm{ex}}^{\star}$	$R_{\mathrm{ex}}^{\max}$ (bit/s/Hz)	$K_s = 1$	$K_s = 2$	$K_s = 5$	$K_s = 10$	$K_s = 15$	$K_s = 30$
			$(\epsilon_\gamma, \epsilon_R^{\mathrm{sur}})$ (%)					
Fitted baseline	6.146	1.829	(38.6, 5.32)	(32.0, 3.47)	(19.8, 1.22)	(3.0, 0.03)	(13.6, 0.50)	(59.4, 8.47)
$K = 15$	5.623	1.813	(32.9, 4.35)	(25.7, 2.51)	(12.3, 0.53)	(6.0, 0.11)	(24.2, 1.66)	(74.2, 12.94)
$K = 50$	5.955	1.826	(36.6, 4.94)	(29.9, 3.10)	(17.2, 0.94)	(0.1, 0.00)	(17.3, 0.81)	(64.5, 9.97)
$\Delta = 0.5$	5.224	2.198	(22.1, 2.98)	(2.4, 0.03)	(118.2, 40.48)	(468.7, 99.94)	(1085.8, 100.00)	(5275.5, 100.00)
$\Delta = 1$	7.048	1.774	(48.6, 10.27)	(48.0, 9.95)	(53.2, 12.83)	(59.7, 17.22)	(63.2, 20.08)	(68.1, 24.65)
$m_1 = 2$	5.356	1.739	(32.7, 4.73)	(29.4, 3.74)	(25.8, 2.79)	(25.2, 2.67)	(25.5, 2.74)	(26.3, 2.92)
$m_1 = 20$	6.375	1.838	(40.3, 5.74)	(33.2, 3.72)	(18.2, 1.03)	(8.9, 0.22)	(43.1, 4.56)	(182.8, 72.96)
$m_2 = 10$	5.975	1.833	(36.8, 4.88)	(29.9, 3.03)	(16.5, 0.84)	(0.6, 0.00)	(16.3, 0.70)	(55.0, 7.24)
$m_2 = 100$	6.167	1.829	(38.8, 5.38)	(32.3, 3.53)	(20.2, 1.27)	(3.5, 0.03)	(13.4, 0.48)	(60.2, 8.70)

K_s	0	1	2	5	10	15	20
$\Delta = 0.5$	(34.5, 7.75)	(22.1, 2.98)	(2.4, 0.03)	(118.2, 40.48)	(468.7, 99.94)	(1085.8, 100.00)	(2048.7, 100.00)
$\Delta = 1$	(51.4, 11.79)	(48.6, 10.27)	(48.0, 9.95)	(53.2, 12.83)	(59.7, 17.22)	(63.2, 20.08)	(65.5, 22.07)

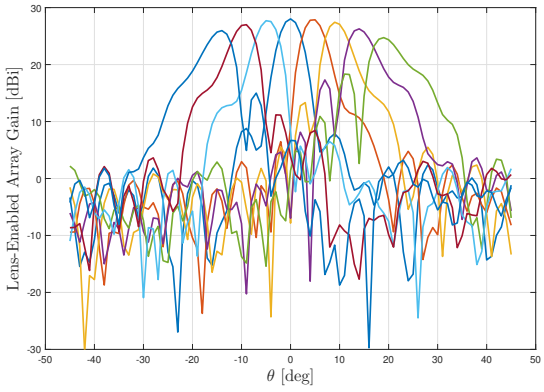


Figure 3: Full-wave lens radiation patterns for the eight feed positions at 28 GHz.

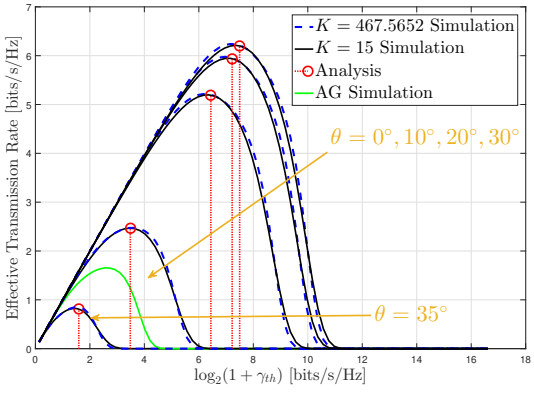


Figure 4: ETR versus fixed transmission spectral efficiency at $\rho = 0$ dB. Markers denote the asymptotic design with $K_s = 15$.

gain. The high-SNR OP yields a closed-form Lambert-W threshold, and the moving-threshold analysis establishes that its normalized argument still tends to zero as the SNR increases.

The exact Gamma-mixture distribution provides a finite-SNR benchmark without assuming a unique ETR maximizer. The second-order OP expansion identifies the first correction omitted by the asymptotic rule. The local loss result further shows why threshold accuracy and ETR accuracy can differ: a small relative threshold error produces an ETR loss proportional to its square, with a coefficient determined by the peak curvature. The numerical perturbation test agrees with this dependence.

For the fitted extreme-K channel, a fixed design surrogate $K_s = 15$ limits ETR loss to below 2.5% at the tested average received SNRs from 0 to 30 dB. All such losses are evaluated on the original physical channel. This accuracy does not transfer uniformly to other IFTR parameters. At $\bar{\gamma} = 10$ dB, choosing $K_s = 2$ reduces the loss to about 0.03% for $\Delta = 0.5$, but the best tested loss for $\Delta = 1$ remains about 9.95%. These results support adapting the surrogate to the channel while also showing the limits of adjusting K_s alone.

With the full-wave patterns of the fabricated lens, the eight-feed example at a transmit SNR of 0 dB exceeds the normalized ideal AG reference within approximately ±30°, with a boresight ETR ratio above three. This gain is specific to the realized lens aperture and the stated equal-power reference.

A. Proof of Lemma 1

Consider the generic instantaneous SNR $\gamma = \bar{\gamma}|\alpha|^2$, where $\bar{\gamma}$ is the average received SNR. From the exact Gamma-mixture CDF in (29), the $j = 0$ component is $A_0(1 - \exp(-z)) = A_0 z + \mathcal{O}(z^2)$ with $z = (1 + K)\gamma_{th}/\bar{\gamma}$, whereas all $j \geq 1$ components start at order z^2 or higher. Hence, the leading term recovers the high-SNR asymptotic OP reported in [15]:

$$\begin{aligned} &P_{\mathrm{out}}(\gamma_{th}) \\ &= \Pr\left\{\bar{\gamma}|\alpha|^2 \leq \gamma_{th}\right\} = \Pr\left\{|\alpha|^2 \leq \frac{\gamma_{th}}{\bar{\gamma}}\right\} \\ &= \Theta\gamma_{th} + \mathcal{O}(z^2), \end{aligned} \tag{56}$$

where Θ is defined in (21). More generally, Proposition 2 gives a remainder of order $\mathcal{O}(z^2)$ after the leading term. For fixed γ_{th} this becomes $\mathcal{O}(\bar{\gamma}^{-2})$. Substituting the leading-order OP into the ETR gives the asymptotic threshold optimization

$$\gamma^{\star}_{th,\mathrm{asy}} = \arg\max_{\gamma_{th}>0} \Big[1 - \Theta\gamma_{th}\Big] \log_2(1+\gamma_{th}). \tag{57}$$

Define $f(\gamma) \triangleq \big[1-\Theta\gamma\big]\log_2(1+\gamma)$ for $\gamma > 0$. Then, the first derivative of $f(\gamma)$ w.r.t. γ is

$$f'(\gamma) = -\Theta \log_2(1+\gamma) + \frac{1-\Theta\gamma}{(1+\gamma)\ln 2}. \tag{58}$$

Setting $f'(\gamma) = 0$ yields

$$\frac{1-\Theta\gamma}{1+\gamma} = \Theta \ln(1+\gamma). \tag{59}$$

Let $u = 1+\gamma$. Rearranging (59) gives $u[1+\ln u] = (1+\Theta)/\Theta$. With $v = 1 + \ln u$, this becomes $v\exp(v) = e(1+\Theta)/\Theta$, so that $v = W(e(1+\Theta)/\Theta)$. Back-substitution gives the unique stationary point

$$\gamma^{\star} = \frac{1+\Theta}{\Theta\, W\big(\frac{e(1+\Theta)}{\Theta}\big)} - 1, \tag{60}$$

where $W(\cdot)$ denotes the Lambert W function [23].

For global optimality, define $g(\gamma) = \frac{1-\Theta\gamma}{1+\gamma} - \Theta\ln(1+\gamma)$, where $g(0) = 1 > 0$ and as $\gamma \to \infty$, we have $g(\gamma) \to -\infty$. Then, we can write the first derivative of $g(\gamma)$ with respect to γ as

$$g'(\gamma) = -\frac{\Theta+1}{(1+\gamma)^2} - \frac{\Theta}{1+\gamma} < 0. \tag{61}$$

Therefore, the equation $f'(\gamma) = 0$ has a unique solution at which $f'(\gamma)$ changes from positive to negative. Hence $\gamma^{\star}$ in (60) is the global maximizer of $f(\gamma)$. Moreover, (59) implies $1 - \Theta\gamma^{\star} > 0$, and therefore $0 < \gamma^{\star} < 1/\Theta$. Thus, the optimizer lies in the region where the asymptotic success-probability factor $1-\Theta\gamma$ remains positive.

Finally, as $\Theta \to 0$, the argument of $W(\cdot)$ diverges. Using the leading large-argument relation $W(x) = \ln x - \ln\ln x + o(1)$ shows that $W(e(1+\Theta)/\Theta) = (1 - \ln\Theta)[1 + o(1)]$. Substitution into (60) yields the leading-order expression (23).

CRediT authorship contribution statement

Hui Zhao: Conceptualization, Methodology, Formal analysis, Writing - original draft. **T. Q. Khai Nguyen:** Validation, Writing - review & editing. **Dirk Slock:** Conceptualization, Supervision, Writing - review & editing.

Acknowledgment

This work was supported in part by EURECOM's industrial members: ORANGE, BMW, SAP, iABG, Norton LifeLock, in part by the EU H2030 project CONVERGE, in part by the French projects EEMW4FIX (ANR21-CE24-0028), PERSEUS (ANR-22-PEFT-0004), and YACARI (ANR-22-PEFT-0005), and in part by the Huawei France-funded Chair toward Future Wireless Networks.

References

[1] S. Sambhwani, H. Chae, S.-E. Chiu, B. Fan, I. Sarkas, W. Sun, J. Zhou, X. Zhu, Extending mmWave deployment in the next-generation network: Coverage and reliability enhancements, IEEE Wireless Commun. 32 (2025) 83–89.

[2] H. Zhao, J. Zhang, L. Yang, G. Pan, M.-S. Alouini, Secure mmWave communications in cognitive radio networks, IEEE Wireless Commun. Lett. 8 (2019) 1171–1174.

[3] R. Méndez-Rial, C. Rusu, N. González-Prelcic, A. Alkhateeb, R. W. Heath, Hybrid MIMO architectures for millimeter wave communications: Phase shifters or switches?, IEEE Access 4 (2016) 247–267.

[4] K. Qu, S. Guo, J. Ye, H. Zhao, Two-stage beamspace music-based near-field channel estimation for hybrid XL-MIMO, IEEE Commun. Lett. 28 (2024) 1949–1953.

[5] K. Qu, K. Pang, H. Zhao, A. Elzanaty, S. Guo, Distance-aware beamspace modulation for near-field spectral efficiency improvement, IEEE Wireless Commun. Lett. 14 (2025) 636–640.

[6] J. Borras, F. Molina, R. López-Valcarce, J. Sala-Álvarez, G. Vazquez, Robust energy-efficient analog beamforming under short packets and per-antenna power constraints, IEEE Trans. Wireless Commun. 24 (2025) 7892–7907.

[7] Z. Wang, Q. Liu, M. Li, and W. Kellerer, Energy efficient analog beamformer design for mmWave multicast transmission, IEEE Trans. Green Commun. Netw. 3 (2019) 552–564.

[8] A. Arora, C. G. Tsinos, M. R. B. Shankar, S. Chatzinotas, B. Ottersten, Efficient algorithms for constant-modulus analog beamforming, IEEE Trans. Signal Process. 70 (2022) 756–771.

[9] Y. Rahmat-Samii, J. Wang, A. Papathanasopoulos, The evolution of printed lens and transmitarray antennas: Navigating representative past, present, and future designs and manufacturing techniques, IEEE Antennas Propag. Mag. 66 (2024) 52–67.

[10] M. Karabacak, H. Arslan, G. Mumcu, Lens antenna subarrays in mmwave hybrid MIMO systems, IEEE Access 8 (2020) 216634–216644.

[11] L. Afeef, G. Mumcu, H. Arslan, Energy and spectral-efficient lens antenna subarray design in mmwave MIMO systems, IEEE Access 10 (2022) 75176–75185.

[12] Y. Zeng, R. Zhang, Millimeter wave MIMO with lens antenna array: A new path division multiplexing paradigm, IEEE Trans. Commun. 64 (2016) 1557–1571.

[13] J. M. Romero-Jerez, F. J. Lopez-Martinez, J. F. Paris, A. J. Goldsmith, The fluctuating two-ray fading model: Statistical characterization and performance analysis, IEEE Trans. Wireless Commun. 16 (2017) 4420–4432.

[14] M. K. Samimi, G. R. MacCartney, S. Sun, and T. S. Rappaport, 28 GHz millimeter-wave ultrawideband small-scale fading models in wireless channels, in: Proc. IEEE 83rd Veh. Technol. Conf. (VTC Spring), 2016, pp. 1–6.

[15] M. Olyaee, J. A. Cortés, F. J. Lopez-Martinez, J. F. Paris, J. M. Romero-Jerez, The fluctuating two-ray fading model with independent specular components, IEEE Trans. Veh. Technol. 72 (2023) 5533–5545.

[16] H. Zhao, Z. Liu, M.-S. Alouini, Different power adaption methods on fluctuating two-ray fading channels, IEEE Wireless Commun. Lett. 8 (2019) 592–595.

[17] H. Zhao, L. Yang, G. Pan, M.-S. Alouini, Secrecy outage analysis over fluctuating two-ray fading channels, Electron. Lett. 55 (2019) 866–868.

[18] J. Zheng, J. Zhang, S. Chen, H. Zhao, B. Ai, Wireless powered UAV relay communications over fluctuating two-ray fading channels, Phys. Commun. 35 (2019) 100724.

[19] P. V. Trinh, S. Sugiura, Maximum secrecy throughput analysis of practical ris-aided mmwave systems over unified FTR/IFTR fading channels, IEEE Trans. Wireless Commun. 23 (2024) 16590–16605.

[20] M. Olyaee, H. Hashemi, J. M. Romero-Jerez, A tractable statistical representation of IFTR fading with applications, IEEE Trans. Commun. 72 (2024) 4677–4691.

[21] M. Nasimi, S. Singh, A. K. Brar, Effective rate analysis of MISO systems over independent fluctuating two-ray fading channels, AEU - Int. J. Electron. Commun. 217 (2026) 156605.

[22] E. Kim, I. P. Roberts, J. G. Andrews, Downlink analysis and evaluation of multi-beam LEO satellite communication in shadowed Rician channels, IEEE Trans. Veh. Technol. 73 (2024) 2061–2075.

[23] I. S. Gradshteyn, I. M. Ryzhik, Table of integrals, series, and products, seventh ed., Academic press, 2007.

[24] H. Zhao, A. Bazco-Nogueras, P. Elia, Coded caching in land mobile satellite systems, in: Proc. IEEE Int. Conf. Commun. (ICC), 2022, pp. 4571–4576.

[25] W. Shang, Z. Xiang, P. Ren, L. Yang, An exact analysis on security-reliability tradeoff in downlink rate splitting multiple access, IEEE Commun. Lett. 29 (2025) 1102–1106.

[26] T. Q. K. Nguyen, F. Ferrero, T. Q. V. Hoang, E. Vandelle, S. Wane, P. Ratajczak, D. Slock, Phased array combined with 3D-printed dielectric lens for millimeter wave fixed wireless access, in: Proc. IEEE Int. Symp. Phased Array Syst. Technol. (ARRAY), 2024, pp. 1–6.